# Chapter 6

# Thermo-mechanical Validation

The further aim of this research is to include material non-linearity within a FV framework, enabling the simulation of complex industrial processes involving not only solid mechanical behaviour, but also other complex physical behaviour such as heat transfer, solidification and fluid dynamics. A case in point is the casting of metals, which involves a wide variety of physical behaviour including that previously described.

The original FV framework upon which this research is based was restricted to two dimensional analyses and was developed as the engineering software UIFS (Unstructured Integrated Fluids and Solids) at the University of Greenwich [42, 20, 22, 26, 25]. The inclusion of material non-linearity within this framework to improve the simulation of a metal casting process is described by Taylor et al [89].

The FV framework has now been extended to the three dimensional engineering software framework PHYSICA [24], also developed at the University of Greenwich. The inclusion of material non-linearity within this framework will be described in this Chapter as it also applies generally to the two dimensional case.

The implementation and the methods employed in the heat transfer, solidification and fluid flow algorithms are those developed at the University of Greenwich by Chow et al [20, 25]. They will not be described in detail in this thesis as they are the results of prior research.

Though it is important to note that for heat transfer, solidification and fluid flow algorithms that exist within PHYSICA at present, a cell-centred FVM as discussed in Chapter 1 is employed.

## 6.1 Conservation equations

The additional equilibrium equations governing the conservation of heat transfer and fluid flow in three dimensions are described as follows:

For momentum

$$\begin{aligned} \frac{\partial \rho U}{\partial t} + \nabla(\rho \mathbf{V} U) &= \nabla.(\mu \nabla U) - \frac{\partial p}{\partial x} + S_U, \\ \frac{\partial \rho V}{\partial t} + \nabla(\rho \mathbf{V} V) &= \nabla.(\mu \nabla V) - \frac{\partial p}{\partial y} + S_V, \\ \frac{\partial \rho W}{\partial t} + \nabla(\rho \mathbf{V} W) &= \nabla.(\mu \nabla W) - \frac{\partial p}{\partial z} + S_W, \end{aligned} \tag{6.1}$$

for continuity

$$\frac{\partial \rho}{\partial t} + \nabla.(\rho \mathbf{V}) = 0, \tag{6.2}$$

and for energy

$$\frac{\partial \rho h}{\partial t} + \nabla(\rho \mathbf{V} h) = \nabla.\left(\frac{k}{c}\nabla h\right) + S_h. \tag{6.3}$$

Where $\mathbf{V} = (U, V, W)$ is the fluid velocity vector, $p$ is the pressure, $h$ is the enthalpy and $\rho, \mu, c$ and $k$ are the material density, viscosity, specific heat and thermal conductivity, respectively.

The source terms $S_U, S_V, S_W$ and $S_h$ contain the additional source terms necessary for the modelling of the solidification process.

For momentum these sources are; buoyancy, to characterize the natural convection of the molten material as it cools and Darcy, to terminate the velocity components as the material

solidifies. For the energy equation the latent heat source, $S_T$, depicts the energy release during the phase change. If the specific heat $c$ is constant, the relationship between enthalpy $h$ and temperature $T$ simplifies to

$$h = cT$$

which upon substitution in equation 6.3 provides

$$\frac{\partial \rho T}{\partial t} + \nabla(\rho \mathbf{V} T) = \nabla . \left(\frac{k}{c} \nabla T\right) + \frac{S_h}{c}. \tag{6.4}$$

In this manner, temperature is chosen as the dependent variable of the energy equation to emphasise the thermo-mechanical coupling via the temperature field.

## 6.2 Thermo-mechanical coupling

The coupling between the thermal and the mechanical analysis is mainly unidirectional via the temperature field. The coupling can occur at an incremental or iterative level, for strongly coupled systems iterative coupling is a necessity. For thermo-mechanical problems involving large plastic strains considerable heat loss can occur as described in section 2.1.1.2, the coupling is then bidirectional and can be performed at an iterative level [99]. Only small strain problems are considered in this research and the heat loss due to plastic straining can be neglected without any reasonable loss of accuracy. For small strain thermo-mechanical problems which have relatively weak coupling, incremental coupling is possible. At an incremental level the thermal analysis is performed over a suitable number of time steps and then the mechanical analysis is performed, this staggered approach is then continually repeated for the complete analysis.

It is important to note that the application of the thermal load in an incremental fashion is essential to capture the path dependent non-linear material behaviour. The geometry may or may not be updated with regard to the thermal analysis, for some problems involving small strains little accuracy is lost by not updating the geometry. Hence, in some cases the thermal and mechanical analysis can be performed separately. For complex applications, such as the die casting of metals, the geometry must be updated with regard to the thermal analysis in order to model the forming of gaps between the cast and mould as deformation

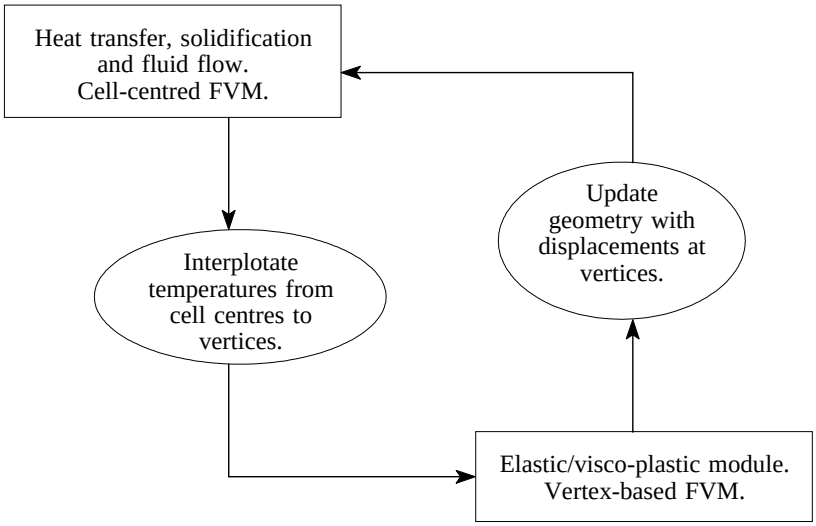


Figure 6.1: Incremental thermo-mechanical coupling within the FV framework.

occurs [12, 67, 42, 68, 63]. The coupling is now bidirectional and for this reason a complete thermo-mechanical coupling of the temperature field and geometry as illustrated in Figure 6.1 is provided within the FV framework PHYSICA [24]. This is equivalent to the original coupling method as employed by Cross et al [26] in the engineering software UIFS.

### 6.2.1 Test case 1: Quenching of a steel slab

This test case involves the quenching of a large steel plate and the consequential residual stress. If interest is restricted to the regions away from the edges of the plate, a plate of infinite extent can be assumed. For a plate of infinite extent, the heat conduction analysis associated with a convective cooling boundary condition at the surfaces is one dimensional and a thermal gradient exists in one direction only, through the thickness of the plate.

The heat flux due to the convective cooling is

$$q = h_c(T - T_A),$$

where $h_c$ is the heat transfer coefficient and $T_A$ is the ambient temperature of the surrounding fluid. The material properties associated with the thermal analysis are described in Table 6.1.

| $\rho$ | $k$ | $c$ | $h_c$ | $T_A$ |
|---|---|---|---|---|
| 7832 $\text{kgm}^{-3}$ | 58.8 W/(mK) | 600 J/(kgK) | 193.1 $\text{W/(m}^2\text{K)}$ | 70 °C |

Table 6.1: Material properties associated with the thermal analysis.

The plate consists of an elastic/perfectly plastic material with a temperature dependent yield stress, as described in Table 6.2. It should be noted that the time dependent stresses are large enough to cause plastic deformation and hence residual stresses will remain after the plate has cooled. The remaining material properties associated with the mechanical

| Temperature (°C) | 70.0 | 121.0 | 1121.0 |
|---|---|---|---|
| Yield stress (MPa) | 248.2 | 248.2 | 24.82 |

Table 6.2: Temperature dependent yield stress.

analysis are described in Table 6.3. The plate is initially at a very high uniform temperature $T_i = 1038°\,\text{C}$, close to the melting point of the material. The plate then cools to the ambient temperature associated with the convective boundary condition.

#### 6.2.1.1 Reference solution

The reference solution is obtained from a semi-analytical method, where an elasto-plastic behaviour with a Von-Mises yield criterion is assumed for the mechanical analysis [62]. The governing differential equations are manipulated in such a way that a numerical step-by-

| $E$ | $\nu$ | $\alpha$ | $\gamma$ | $H$ |
|---|---|---|---|---|
| $2.068 \times 10^5$ MPa | 0.3 | $1.35 \times 10^{-5}$ /K | $1.0 \times 10^{-4}$ /s | 0 MPa |

Table 6.3: Material properties associated with the mechanical analysis.

step procedure can be performed with regard to time, where the temperature, stress and location of the plastic regions at time $t+\Delta t$ are computed from values at time t. An explicit finite difference technique is employed with regard to temperature, but an implicit finite difference technique is employed with regard to the solid mechanics [62].

#### 6.2.1.2 Numerical analysis

The numerical analysis is performed in three dimensions using the engineering software PHYSICA [24]. One of the meshes employed in the analysis is illustrated in Figure 6.2 and consists of 40 TLH elements. With regard to the mechanical and thermal analysis within the FV framework, it is important to note that mesh elements are conceptually different at present. With regard to the thermal analysis the cell-centred FVM employed allows an

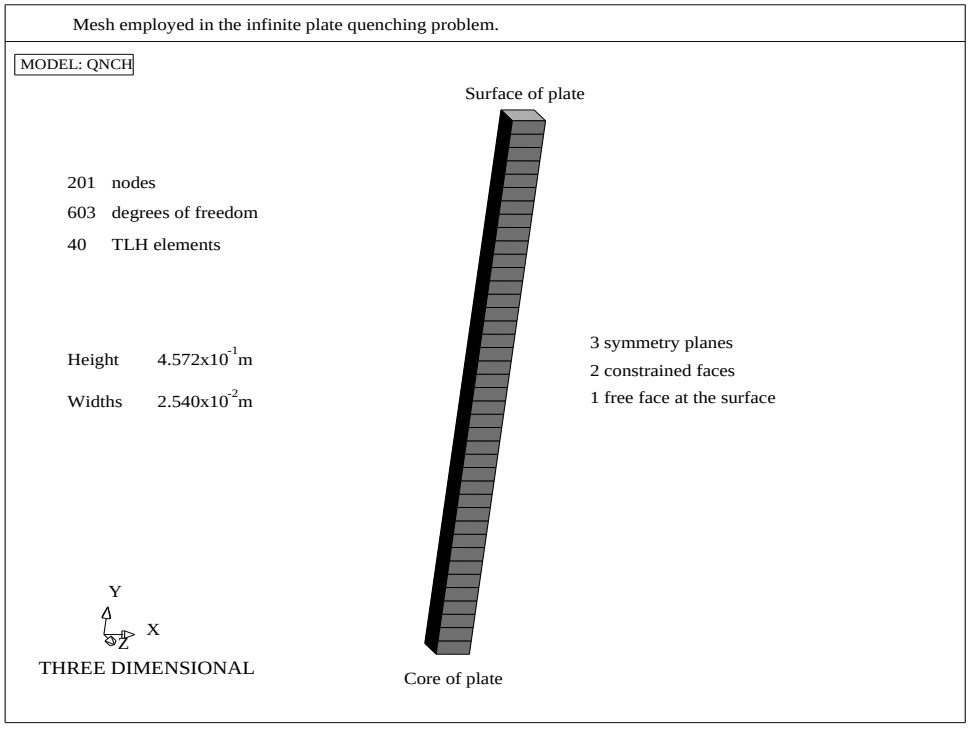


Figure 6.2: Quenching of an infinite steel plate.

arbitrary polygon to be employed as an element in the mesh, thus any element selected for a mechanical analysis is compatible with the thermal analysis [24, 20]. Thus allowing the

simulation of complex geometries with irregular meshes. Though it is important to note that any non-orthogonality and non-conjuctionality present can introduce mesh effects into the thermal analysis [24]. Methods have been developed to overcome these difficulties [24, 20]. Such problems involving complex geometries will be modelled in the following chapter.

For the mechanical analysis a state of generalized plane strain is assumed [58], such that

$$\sigma_{xy} = \sigma_{yz} = \sigma_{zx} = 0,$$

$$\sigma_{xx} = \sigma_{zz},$$

$$\sigma_{yy} = 0.$$

This is achieved using constraint equations as described in Appendix E. The nodes on the free faces in the $x$ and $z$ planes, as illustrated in Figure 6.2, are constrained to translate with the same displacement in the $x$ and $z$ directions, respectively. This is achieved by assigning a master degree of freedom to slave degrees of freedom on the relevant faces. The transient thermal analysis is performed with a gradually increasing time step. The mechanical analysis is performed at every ten time steps of the thermal analysis and in this way the thermal load is applied in an incremental fashion, which captures the path dependent mechanical behaviour. It is important to note that the elasto-visco-plastic analysis converges to a steady state solution during each mechanical analysis and is equivalent to an inviscid elasto-plastic solution [105].

Additionally, a numerical reference solution is available using the FE engineering software LUSAS [36]. This problem is described in the LUSAS verification manual [36] and is available as an example case. In LUSAS the numerical analysis is performed using a two dimensional axisymmetric approximation and the mesh consists of ten bi-quadratic quadrilateral elements [36]. The results obtained using LUSAS are illustrated in Figure 6.6.

#### 6.2.1.3 Discussion of numerical results

The transient behaviour of the mechanical analysis is illustrated in Figure 6.3. The transient stress and plastic strain behaviour at the core, mid-point and surface of the plate are illustrated in Figures 6.3.1 and 6.3.3.

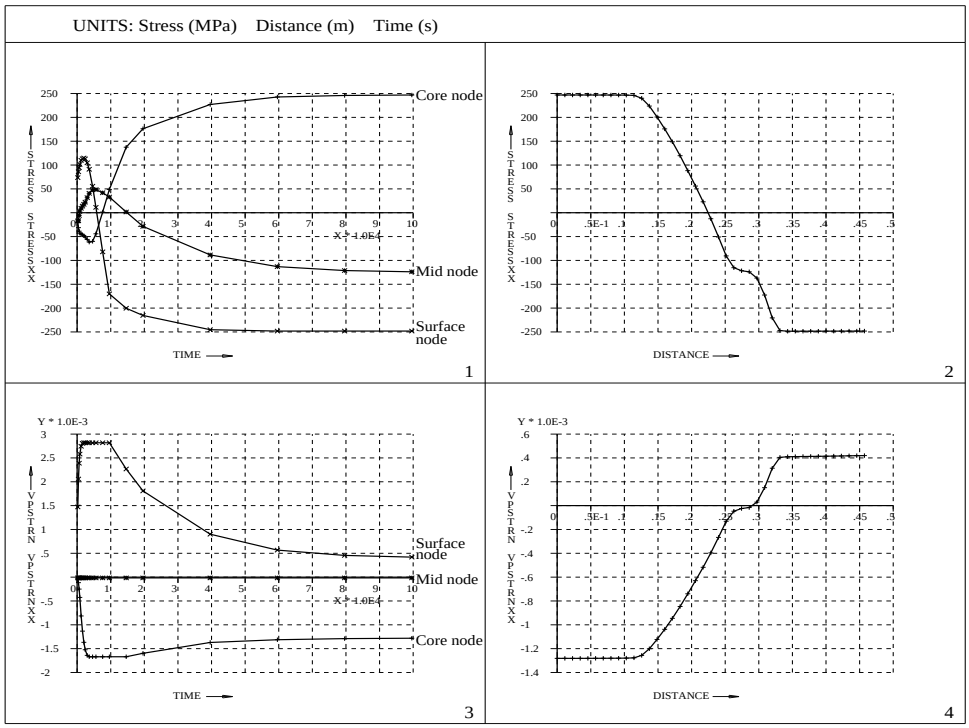


Figure 6.3: Transient behaviour of stress and plastic strain during quenching.

From the stress behaviour it is possible to observe the stress reversal phenomenon associated with the quenching problem. Initially the stress at the surface is tensile, but at the end of the analysis the residual stress is compressive, the opposite is true for the core. From the plastic strain behaviour it is possible to observe a mid-point region which is permanently elastic and does not undergo any plastic straining during the quenching. The residual stresses are illustrated in Figure 6.3.2 and the associated plastic strains are illustrated in Figure 6.3.4.

The numerical analysis was performed with PHYSICA using a fine mesh involving 40 TLH elements as illustrated in Figure 6.2 and a coarser mesh involving 9 TLH elements. The results from the coarse mesh are illustrated in Figure 6.4 and compare well with the reference solution and the numerical analysis performed in LUSAS, which is illustrated in Figure 6.6.

Though it is important to note, that to capture the purely elastic behaviour in the mid-

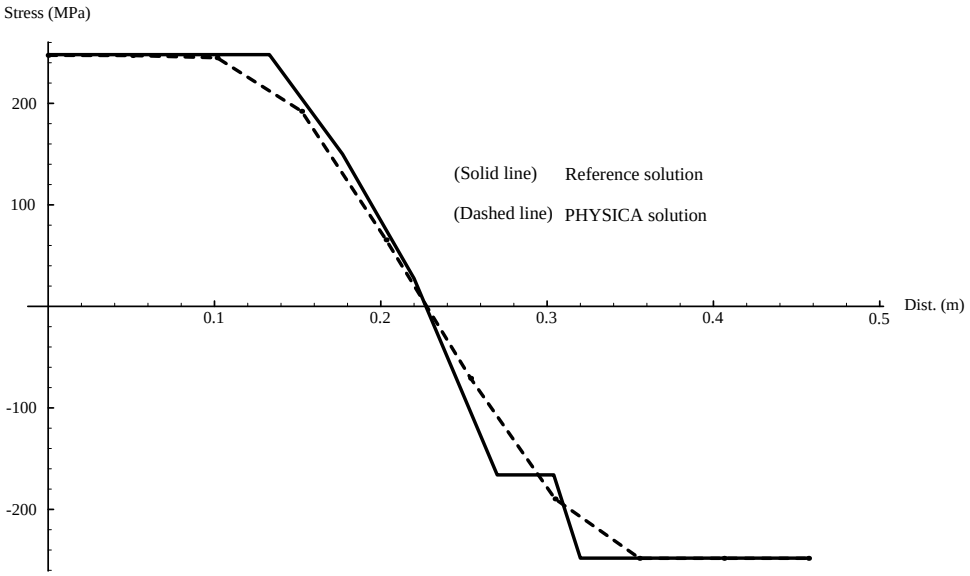


Figure 6.4: Residual stress after quenching (coarse mesh).

point region a finer mesh is required. This is illustrated in Figure 6.5, where the residual stresses are much closer to those of the reference solution.

In closure, it should be noted that for this problem the heat transfer coefficient $h_c$ associated with the convective boundary condition is constant and was selected to resemble quenching in air. Further research has been performed on quenching in liquids such as water and temperature dependent heat transfer coefficients have been employed [58]. Also the Leidenfrost phenomenon can be included, which accounts for the formation of vapour blankets around the quenched component, severely effecting the cooling rate [40, 39]. Finally, for metals such as steels, crystal transformations can occur during the quenching process which will then contribute to the total strains. Such phenomena has been studied elsewhere, extensively, and is noted in this research as a point of interest [1].

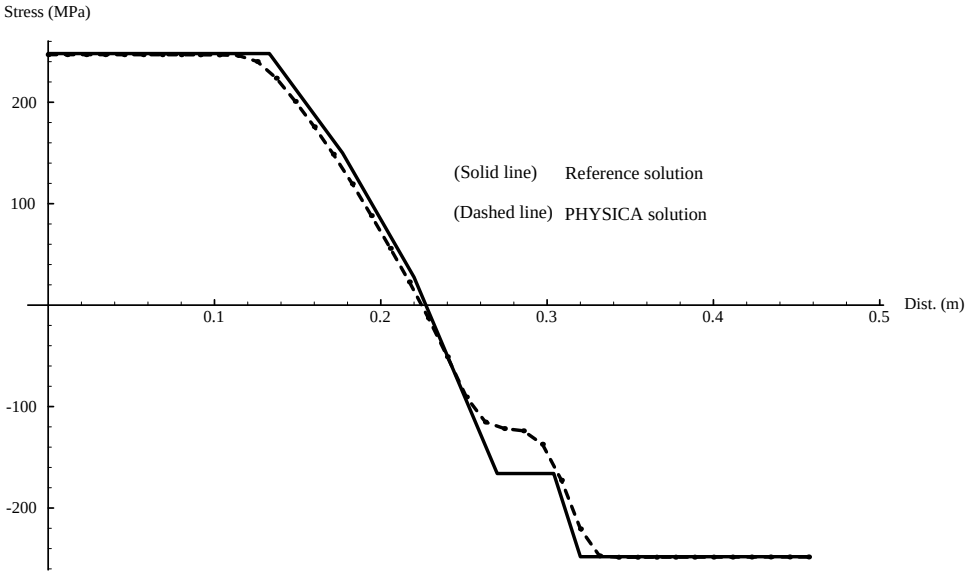


Figure 6.5: Residual stress after quenching (fine mesh).

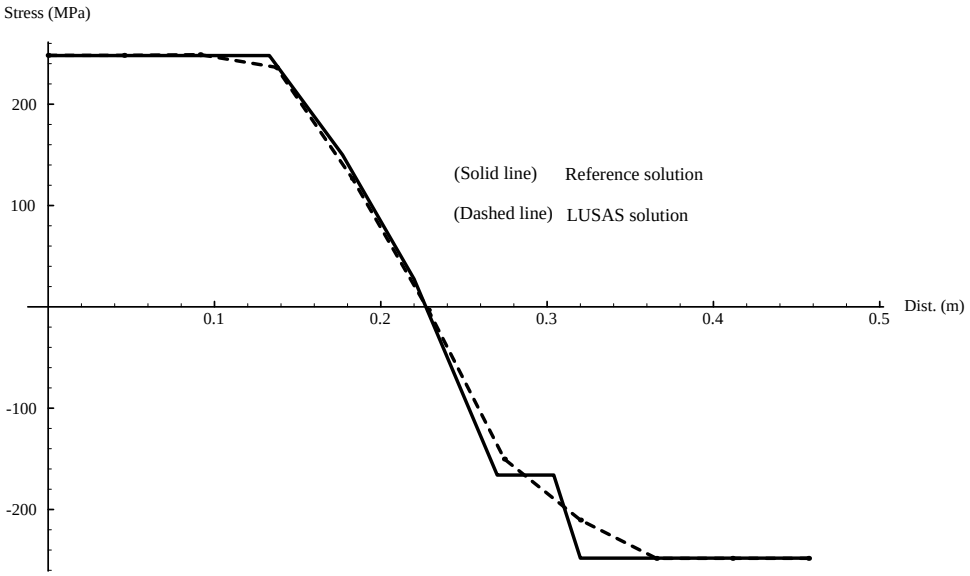


Figure 6.6: Residual stress after quenching.

### 6.2.2 Test case 2: Solidification of a steel slab

This validation problem is an extension of the previous problem. In this case the slab is initially liquid and is assumed to solidify by heat conduction only. The heat conduction analysis is simplified by assuming a fixed temperature at the surface. This validation problem has been studied by a number of researchers employing a variety of commercial FE software [95, 60].

The geometrical approximation of an infinite slab as described in Figure 6.2 can also be assumed in the modelling of the continuous casting of steel [60]. Where the geometry represents a slice of the cross-section of a casting strand. In this case the dimensions of the problem are length, 8mm and widths, 1mm and the mesh consists of 40 TLH elements. The thermal boundary conditions and material properties can be modified to represent different types of steel under various cooling conditions [60].

#### 6.2.2.1 Analytical solution

A commonly referenced analytical solution is available for this problem [98]. The analytically derived equations will be stated here for completeness. With regard to the one dimensional thermal analysis the position of the solidification front at any time $t$ is

$$x_s = 2\lambda\sqrt{\frac{kt}{\rho c}}, \tag{6.5}$$

where the constant $\lambda$ is the solution of the following equation:

$$\frac{1}{e^{\lambda^2}\,\mathrm{Erf}(\lambda)} - \frac{T_l - T_s}{e^{\lambda^2}\,T_s\,(1-\mathrm{Erf}(\lambda))} = \frac{h\,\lambda\,\sqrt{\pi}}{c\,T_o} \tag{6.6}$$

and the temperatures $T_s$, $T_l$ and $T_o$ denote the solidus, liquidus and initial temperature drop at the surface, respectively [17]. The error function $\mathrm{Erf}(\lambda)$ is defined in Appendix A and $h$ is the latent heat per unit mass. Initially at time $t = 0$, the slab is at the liquidus temperature and the temperature at the surface is dropped to $T_s = 1300^{\circ}$C and kept constant thereafter. Using the material properties as described in Table 6.4, equation 6.6 can be solved for $\lambda$, in this case using the commercial software MATHEMATICA [102].

| $T_s$ | $T_l$ | $T_o$ | $h$ | $c$ |
|---|---|---|---|---|
| 1468 °C | 1525 °C | 168 °C | $2.72 \times 10^5$ J/Kg | 700 J/(KgK) |

Table 6.4: Material properties associated with the solidification analysis.

With regard to the theoretical mechanical analysis an assumption of similarity is employed [98], which assumes that the stress solution and hence ratio of the elastic and plastic regions is independent of time. This coincides with temperature distribution which is also independent of time when the equations are cast in a normalized fashion [98].

From the theoretical analysis the following simultaneous equations with respect to $s$ and $t$ are obtained:

$$\begin{aligned} \frac{2\ (1-m)\ s}{e^{s^2}} &= \frac{-\frac{1-m}{e^{s^2}} - \left(1+e^{-\lambda^2}\right)\ m + \frac{1+m}{e^{t^2}}}{s-t}, \\ \frac{2\ (1-m)\ s}{e^{s^2}\sqrt{\pi}} &= \frac{2\,m\,\mathrm{Erf}(\lambda) + (1-m)\ \mathrm{Erf}(s) - (1+m)\ \mathrm{Erf}(t)}{\log(\frac{s}{t})}. \end{aligned}$$

Where

$$m = \frac{(1-\nu)Y_o}{\alpha E T_o}$$

and the ratio of the elastic and plastic regions are defined by the variables $s$ and $t$. It is important to note that the yield stress is assumed to vary linearly, decreasing from $Y_o$ at the surface temperature to zero at the solidus temperature.

| $\nu$ | $Y_o$ | $\alpha$ | $E$ |
|---|---|---|---|
| 0.35 | 20 MPa | $2.0 \times 10^{-5}$ /K | $4.0 \times 10^4$ MPa |

Table 6.5: Material properties associated with the mechanical analysis.

Substituting the material properties as described in Table 6.5 into the above simultaneous equations and solving for $s$ and $t$ using MATHEMATICA [102], the following values can be obtained:

$$s = 0.218068, \qquad t = 0.0830676.$$

The stress distribution is described by the following three equations [98]:

$$\sigma(x) = m\left(1 - \frac{\mathrm{Erf}(\lambda\, x)}{\mathrm{Erf}(\lambda)}\right) \qquad \text{for} \quad s' < x < 1, \qquad (6.7)$$

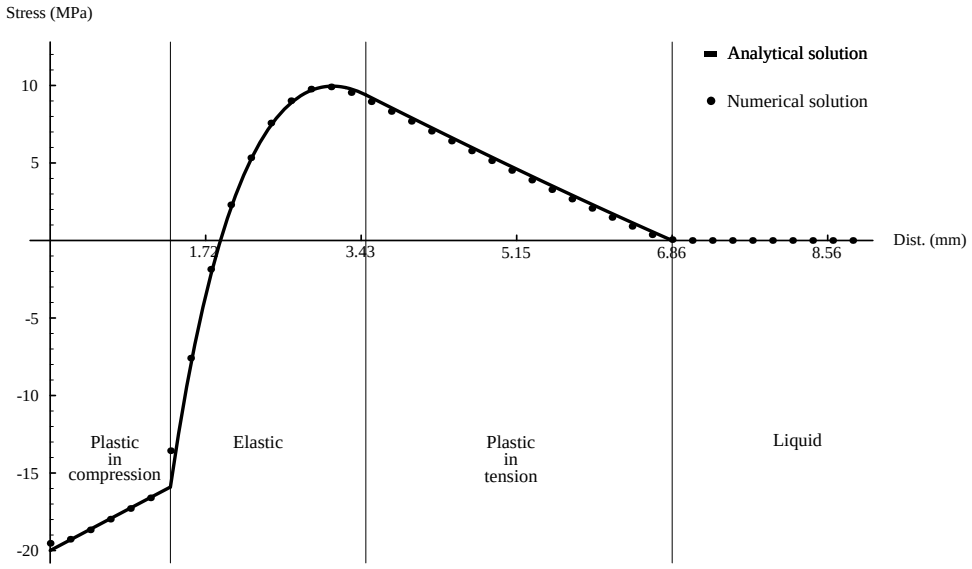


Figure 6.7: Stress distribution after 10s of solidification.

$$\sigma(x) = m\left(1-\frac{\mathrm{Erf}(s)}{\mathrm{Erf}(\lambda)}\right)+\frac{\mathrm{Erf}(s)-\mathrm{Erf}(\lambda\,x)}{\mathrm{Erf}(\lambda)}- \frac{2\,(1-m)\;s\;\log(\frac{s}{\lambda\,x})}{e^{s^2}\,\sqrt{\pi}\,\mathrm{Erf}(\lambda)} \qquad \text{for} \quad t' < x < s', \tag{6.8}$$

$$\sigma(x) = m\left(\frac{\mathrm{Erf}(\lambda\,x)}{\mathrm{Erf}(\lambda)}-1\right) \qquad \text{for} \quad 0 < x < t'. \tag{6.9}$$

Where $s' = \lambda s$ and $t' = \lambda t$. Equations 6.7, 6.8 and 6.9 represent the normalised stress distribution, such that the solidification front is at $x = 1$ and the surface is at $x = 0$. The non-normalized stress distribution can be obtained and is employed as the reference solution in Figure 6.7. Equation 6.7 describes the stress distribution in the compressive plastic range, equation 6.8 describes the stress distribution in the elastic range and equation 6.9 describes the stress distribution in the tensile plastic range [98]. In the theoretical analysis, only the stresses in the growing elastic/perfectly plastic solidified portion of the slab are considered. The stresses in the liquid region are considered zero.

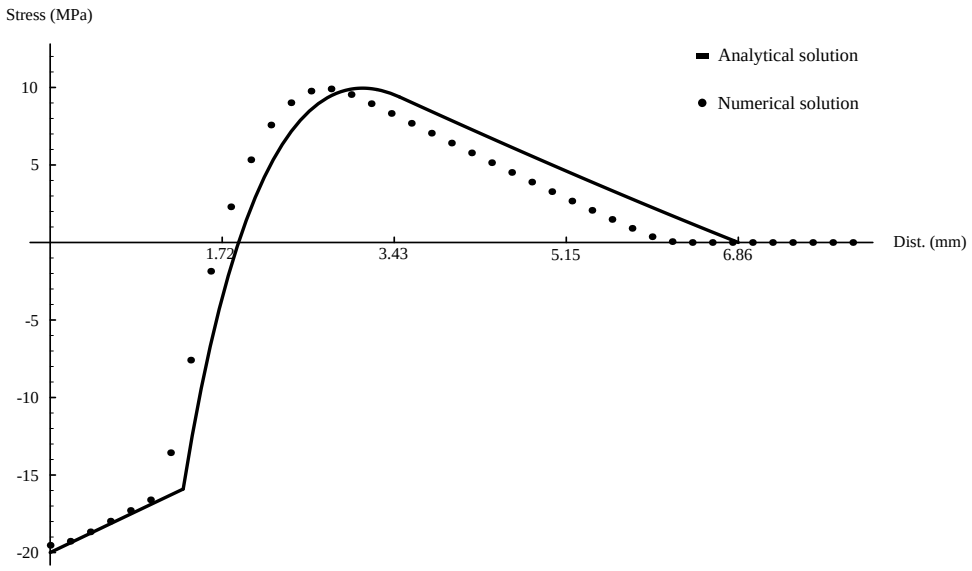


Figure 6.8: Comparison of stress distributions with regard to solidification fronts.

#### 6.2.2.2 Numerical procedure for solidification

The solidification is assumed to occur by heat conduction only. The problem is then simplified considerably, which allowed a theoretical analysis to be performed. With regard to the numerical analysis performed using PHYSICA, a number of correction methods for the liquid fraction update are available [22]. For this problem the default method of Voller and Prakash is employed [79]. This technique is a source based method with regard to solidification. Which casts the problem in a non-linear form, but furnishes a more robust algorithmic approach [97].

#### 6.2.2.3 Numerical procedure for liquid regions

In order to consider the deformation of both liquid and solid regions in the mechanical analysis, a special procedure is required for liquid regions. The procedure adopted for this validation problem is that described by Tszeng and Kobayashi [95]. Other procedures

exist, such as that described by Kristiansson [60], but these methods involve prescribing zero displacements to nodes that exist within liquid regions and can fail to account for hydrostatic pressure acting along the solidification front [95].

In the procedure adopted here, at temperatures greater than the coherence temperature (which is assumed to be equal to the liquidus temperature in this case), a Poisson's ratio very close to 0.5 is artificially assigned. Hence, making the liquid phase close to incompressible for mechanical loads. In order to avoid singularity occurring in the coefficient matrix, a value close to zero is assigned to the Young's modulus. This is equivalent to assigning zero stiffness to liquid regions. In this fashion, values of Poisson's ratio and Young's modulus can be chosen to suppress the deviatoric stress component, whilst allowing a volumetric (or metallostatic) component to exist [95].

#### 6.2.2.4 Numerical analysis

The numerical analysis was performed using PHYSICA and the stress distribution after 10s is illustrated in Figures 6.7 and 6.8. The stress distribution of the theoretical solution is matched to that of the numerical solution with regard to the solidification front in Figure 6.7. In Figure 6.8 the position of the solidification front is calculated using equation 6.5, which assumes a semi-infinite body with regard to the thermal analysis. For the numerical analysis a symmetry condition is assumed at the core of the body with regard to the thermal analysis, this will effect the temperature distribution and hence the prediction of the solidification front in the body, causing disagreement between the theoretical and numerical solution. This is clearly illustrated in Figure 6.8.

In this validation problem the hydrostatic pressure is negligible and the stresses in the liquid region are zero as illustrated in Figures 6.7 and 6.8.

## 6.3 Closure

In this Chapter, the procedures employed to obtain numerical solutions for non-linear, thermo-mechanical problems have been described. The procedures have been validated against a number of test cases involving simple geometries and unidirectional coupling with regard to the thermo-mechanical analysis. In the following Chapter, the procedures will be validated and verified against a number of test cases involving more complex geometry and complete coupling with regard to the thermo-mechanical analysis.